

# MAXI observations of GRBs

Motoko SERINO,<sup>1</sup> Takanori SAKAMOTO,<sup>2</sup> Nobuyuki KAWAI,<sup>3,1</sup> Atsumasa YOSHIDA,<sup>2,1</sup>  
Masanori OHNO,<sup>4</sup> Yuji OGAWA,<sup>5</sup> Yasunori NISHIMURA,<sup>5</sup> Kosuke FUKUSHIMA,<sup>6</sup>  
Masaya HIGA,<sup>7</sup> Kazuto ISHIKAWA,<sup>3</sup> Masaki ISHIKAWA,<sup>8</sup> Taiki KAWAMURO,<sup>9</sup>  
Masashi KIMURA,<sup>10</sup> Masaru MATSUOKA,<sup>1,10</sup> Tatehiro MIHARA,<sup>1</sup> Mikio MORII,<sup>1</sup>  
Yujin E. NAKAGAWA,<sup>11</sup> Satoshi NAKAHIRA,<sup>10</sup> Motoki NAKAJIMA,<sup>12</sup> Yuki NAKANO,<sup>2</sup>  
Hitoshi NEGORO,<sup>6</sup> Takuya ONODERA,<sup>6</sup> Masayuki SASAKI,<sup>13</sup> Megumi SHIDATSU,<sup>9</sup>  
Juri SUGIMOTO,<sup>1</sup> Mutsumi SUGIZAKI,<sup>1</sup> Fumitoshi SUWA,<sup>6</sup> Kazuhiko SUZUKI,<sup>6</sup>  
Yutaro TACHIBANA,<sup>3</sup> Toshihiro TAKAGI,<sup>1,6</sup> Takahiro TOIZUMI,<sup>3</sup> Hiroshi TOMIDA,<sup>10</sup>  
Yohko TSUBOI,<sup>7</sup> Hiroshi TSUNEMI,<sup>13</sup> Yoshihiro UEDA,<sup>9</sup> Shiro UENO,<sup>10</sup> Ryuichi USUI,<sup>3</sup>  
Hisaki YAMADA,<sup>5</sup> Takayuki YAMAMOTO,<sup>1</sup> Kazutaka YAMAOKA,<sup>14,15</sup> Makoto YAMAUCHI,<sup>5</sup>  
Koshiro YOSHIDOME<sup>5</sup> and Taketoshi YOSHII<sup>3</sup>

<sup>1</sup>MAXI team, *Institute of Physical and Chemical Research (RIKEN), 2-1 Hirosawa, Wako, Saitama*  
351-0198

*motoko@crab.riken.jp*

<sup>2</sup>*Department of Physics and Mathematics, Aoyama Gakuin University,*  
5-10-1 Fuchinobe, Chuo-ku, Sagamihara, Kanagawa 252-5258

<sup>3</sup>*Department of Physics, Tokyo Institute of Technology, 2-12-1 Ookayama, Meguro-ku, Tokyo*  
152-8551

<sup>4</sup>*Department of Physical Sciences, Hiroshima University, 1-3-1 Kagamiyama, Higashi-Hiroshima,*  
Hiroshima 739-8516

<sup>5</sup>*Department of Applied Physics, University of Miyazaki, 1-1 Gakuen Kibanadai-nishi, Miyazaki,*  
Miyazaki 889-2192

<sup>6</sup>*Department of Physics, Nihon University, 1-8-14 Kanda-Surugadai, Chiyoda-ku, Tokyo 101-8308*

<sup>7</sup>*Department of Physics, Chuo University, 1-13-27 Kasuga, Bunkyo-ku, Tokyo 112-8551*

<sup>8</sup>*School of Physical Science, Space and Astronautical Science, The graduate University for Advanced*  
*Studies, Yoshinodai 3-1-1, Chuo-ku, Sagamihara, Kanagawa 252-5210*

<sup>9</sup>*ISS Science Project Office, Institute of Space and Astronautical Science (ISAS), Japan Aerospace*  
*Exploration Agency (JAXA), 2-1-1 Sengen, Tsukuba, Ibaraki 305-8505*

<sup>10</sup>*Department of Astronomy, Kyoto University, Oiwake-cho, Sakyo-ku, Kyoto 606-8502*

<sup>11</sup>*ISS Science Project Office, Institute of Space and Astronautical Science (ISAS), Japan Aerospace*  
*Exploration Agency (JAXA), 3-1-1 Yoshinodai, Chuo-ku, Sagamihara, Kanagawa 252-5210*

<sup>12</sup>*School of Dentistry at Matsudo, Nihon University, 2-870-1 Sakaecho-nishi, Matsudo, Chiba*  
101-8308

<sup>13</sup>*Department of Earth and Space Science, Osaka University, 1-1 Machikaneyama, Toyonaka, Osaka*  
560-0043

<sup>14</sup>*Department of Particle Physics and Astronomy, Nagoya University, Furo-cho, Chikusa-ku,  
Nagoya, Aichi 464-8601*

<sup>15</sup>*Solar-Terrestrial Environment Laboratory, Nagoya University, Furo-cho, Chikusa-ku, Nagoya,  
Aichi 464-8601*

(Received ; accepted )

### Abstract

Monitor of all-sky image (MAXI) Gas Slit Camera (GSC) detects gamma-ray bursts (GRBs) including the bursts with soft spectra, such as X-ray flashes (XRFs). MAXI/GSC is sensitive to the energy range from 2 to 30 keV. This energy range is lower than other currently operating instruments which is capable of detecting GRBs. Since the beginning of the MAXI operation on August 15, 2009, GSC observed 35 GRBs up to the middle of 2013. One third of them are also observed by other satellites. The rest of them show a trend to have soft spectra and low fluxes. Because of the contribution of those XRFs, the MAXI GRB rate is about three times higher than those expected from the BATSE  $\log N - \log P$  distribution. When we compare it to the observational results of the Wide-field X-ray Monitor on the High Energy Transient Explorer 2, which covers the the same energy range to that of MAXI/GSC, we find a possibility that many of MAXI bursts are XRFs with  $E_{\text{peak}}$  lower than 20 keV. We discuss the source of soft GRBs observed only by MAXI. The MAXI  $\log N - \log S$  distribution suggests that the MAXI XRFs distribute in closer distance than hard GRBs. Since the distributions of the hardness of galactic stellar flares and X-ray bursts overlap with those of MAXI GRBs, we discuss a possibility of a confusion of those galactic transients with the MAXI GRB samples.

**Key words:** Gamma-ray burst: general — methods: data analysis – X-rays: bursts

## 1. Introduction

X-ray flashes (XRFs) are subclass of gamma-ray bursts (GRBs) which have significantly softer spectra than those of classical GRBs. They are characterized by absence of emission at the high energy band ( $>50$  keV) (Strohmayr et al., 1998; Heise et al., 2001). Later, the empirical classification of GRBs using fluence ratio in the 2–30 keV to 30–400 keV bands was introduced (Sakamoto et al., 2005). While the peak energy values,  $E_{\text{peak}}$ , in the spectra of XRFs distinguish them from classical hard GRBs, Sakamoto et al. (2005) suggest that they arise from the same class based on the HETE-2 samples.

Various models have been proposed to explain the origin of low  $E_{\text{peak}}$  in XRFs. Some of them do not assume intrinsic difference in the source. Instead, the apparent differences to

hard GRBs are caused by the redshift of the sources (Heise et al., 2001) or observer’s viewing angles of the GRB jets (Yamazaki et al., 2002). Others require the intrinsic difference in the conditions of the sources (Mészáros et al., 2002; Zhang & Mészáros, 2002; Lamb et al., 2005). Some of the predictions of those models are investigated against the observed data (Granot et al., 2005; D’Alessio et al., 2006).

Although it is natural to imagine that GRBs which occurred at high redshift have low (apparent)  $E_{\text{peak}}$ , we have not yet observed such an event. So far, all of XRFs with  $E_{\text{peak}}$  lower than 20 keV have relatively low redshift; the redshift values of XRF 020903 ( $E_{\text{peak}} < 5$  keV; Sakamoto et al., 2004), XRF 050416A ( $E_{\text{peak}} = 13.67$  keV; Sakamoto et al., 2006), and XRF 091018 ( $E_{\text{peak}} = 19.43$  keV; Sakamoto et al., 2011) are 0.25 (Soderberg et al., 2004), 0.6528 (Soderberg et al., 2007), and 0.971 (Chen et al., 2009; Wiersema et al., 2012) respectively.

There are some attempts to estimate the luminosity function of GRBs (Butler et al., 2010; Wanderman & Piran, 2010; Qin et al., 2010; Virgili et al., 2011; Lien et al., 2014). However, in order to estimate the luminosity function at high redshift more precisely, it is necessary to observe GRBs at lower energy range to reduce a selection effect. Monitor of All-sky X-ray Image (MAXI) is one of the X-ray instruments which have a capability to observe such an extremely soft GRB and alert its location to the community promptly (Matsuoka et al., 2009).

MAXI is an experimental payload on the exposed facility of Japanese Experiment Module attached to the International Space Station (ISS). It started nominal observation on August 15, 2009, and keep monitoring the X-ray sky since then. MAXI has two scientific instruments: the Gas Slit Camera (GSC; Mihara et al., 2011; Sugizaki et al., 2011) and the Solid-state Slit Camera (SSC; Tsunemi et al., 2010; Tomida et al., 2011). GSC has a larger effective area and field of view (FOV) than those of SSC. Therefore, GSC is suitable to detect GRBs. In this paper, we present the results based on the GSC data. The GRB observations based on the SSC data will be presented elsewhere.

MAXI employs a slit and slat collimator optics. This optics has an advantage over conventional coded-mask systems in reducing the contamination from the cosmic X-ray background to a point source. Therefore MAXI GSC achieves the highest sensitivity as a monitoring instrument in X-ray energy range, so far.

One of the most comprehensive studies of GRBs below 10 keV has been accomplished by Sakamoto et al. (2005). They utilized the data sets observed by the Wide-field X-ray Monitor (WXM; Shirasaki et al., 2003) on the High Energy Transient Explorer 2 (HETE-2; Ricker et al., 2003). We will present here a comprehensive study of the MAXI/GSC GRB samples so that we can compare them with those of WXM.

## 2. Observations and Data Analyses

### 2.1. Gas Slit Camera(GSC)

The GSC consists of 12 one-dimensional position sensitive proportional counters operating in the 2–30 keV range. Because the slit and slat collimator optics has a smaller FOV than that of a coded-mask optics, the cosmic X-ray background of GSC is rather lower than HETE-2/WXM. Two GSC camera units, GSC-H (horizontal camera) and GSC-Z (zenithal camera), have an instantaneous FOV of  $3^\circ \times 160^\circ$  by pointing orthogonal directions each other. GSC covers 70% of the whole sky every orbit.

The GSC counters are only operated within latitude of  $\pm 40^\circ$  to avoid a risk of discharge due to a high particle background that could leave damages on the carbon-anode wires. Because of this restriction, the operation efficiency (i.e. fraction of actual observing time) of GSC is about 40% except for the first 1.5 months (figure 1). The counters which experience a discharge were tentatively stopped or operated by reducing voltage from 1650 V to 1550 V (Sugizaki et al. (2011) in detail). The slight decrease of the sensitivity is expected because of the reduction of the voltage. However, we find no significant difference in the observed rate of GRBs between the periods when the cameras are operated in 1650 V and 1550 V.

MAXI scans a certain celestial position every 92 min that is the orbital period of ISS. A typical transit time on a point source is about 40–100 sec, depending on the source-acquisition angle  $\beta$  (Sugizaki et al., 2011). A typical effective area for a point source is about  $10 \text{ cm}^2$  in the 4–10 keV band. In addition, the effective area to a source varies during a scan, because the position of the source moves in the detector plane. This variation of the effective area during a scan makes it difficult to know intrinsic variation of a source flux. However, we can estimate the uncertainty of the average flux during a scan by the method described in section 2.4.1.

### 2.2. Data reduction and sample selection

We analyzed X-ray event data of the GSC data process version 1.4. Both the data collected in 1650 V and 1550 V were used in the analysis. For analyzing GRBs, we extracted X-ray events within  $10^\circ$  from the best burst position. All the light curves and the spectra were created from these extracted X-ray events.

There are three ways to identify GRBs or other transient events from the MAXI data. First, the transient event can be identified automatically by the search program called *the MAXI Nova-Alert System* (Suwa et al., 2010). Second, the ground search of the MAXI data is possible by knowing the trigger time and the location of GRBs informed by other satellites. Third, we occasionally find transient sources by eye inspection of daily or orbital all-sky images of MAXI.

We selected transient events which had the signal-to-noise ratio (S/N) larger than 5 and only lasted for one scan. If the position of the event matches within 1 degree to a known X-ray

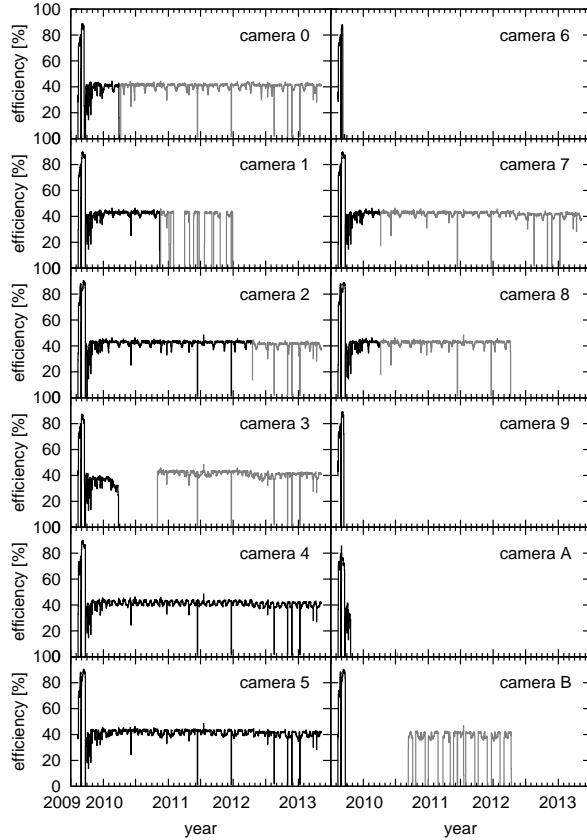


**Fig. 1.** The operation efficiency of GSC counters. The black and gray lines represent the operation with 1650 V and 1550 V, respectively. Two cameras on the same row (e.g., camera 0 and camera 6) cover the same FOV. Loss of either one of the cameras reduces the effective area to a half.

source, we exclude it from our sample. We also excluded the events which had galactic latitude  $b$  between  $\pm 10^\circ$  to avoid contamination from the galactic transients. The only exception is GRB 091230, which has a low galactic latitude but is confirmed as a GRB by INTEGRAL (Gotz et al., 2009).

In table 1, we describe the parameters for 35 GRBs and short X-ray transients observed by MAXI from August 2009 up to April 2013. The explanations of columns of table 1 are following. ‘Time’ is the center time of the transit in which the burst was observed. The transit time depends on the source position. If the positions of the sources are determined by X-ray or optical telescopes accurately (table 2), we used those position. Otherwise we used the position calculated with MAXI data (section 2.3). ‘(RA, Dec)’ is the GRB location calculated with MAXI data in J2000, ‘loc. error’ is error of the position, ‘cameras’ is the camera numbers which observed the GRB, ‘S/N’ is the signal-to-noise ratio of the GRB in the 2–20 keV band, ‘trigger’ is the method that we found the GRB, ‘other sat.’ is other satellites which observed the GRB. The trigger (or detection) time of the instrument from the time in the ‘time’ column are shown in the square brackets. ‘delay’ is the time delay in sending GCN or ATel after the

detection of the bursts.

For the GRBs with X-ray and/or optical afterglows, we summarized information of the counterparts in table 2. ‘Band’ column shows the band of observation of the counterparts. ‘(RA, Dec)’ and error are the GRB location in J2000 and its error determined by the observations of the counterparts. ‘GCN#’ is the number of GCN circular which report the position of X-ray or optical counterparts. ‘Redshift’ is measured redshift (and its reference) of the GRB.

### 2.3. Localization

A point spread function (PSF) of a constant source in the MAXI data can be represented by the product of a spatial distribution in the detector anode direction and the effective area variation in the time direction. For an instantaneous observation, a spatial distribution of the X-ray photons from a point source can be expressed as a Gaussian distribution in the MAXI data. The effective area to a source is expressed as a triangular function of the time. Therefore a PSF of a source can be represented by the product of the Gaussian in the detector anode direction and the triangular function in the time direction.

Figure 2 shows a sample PSF of GSC. An intersection of the PSF for the direction along the detector anode-wire ( $x$ ) is modeled with a Gaussian. An intersection of the PSF for the direction along the scan (i.e. time,  $t$ ) reflects the variation of the effective area during the scan, and thus has the triangular shape.

In order to determine the position of an X-ray source, first we fit the two-dimensional (2-D) PSF to the position histogram of X-ray events in the  $x-t$  plane. Then the position in  $x-t$  plane is converted to the celestial coordinate using the information of the ISS attitude.

During the position fitting process, we fix the width of the Gaussian and the triangles based on the source position at the detector plane. There are three free parameters; the time at the peak, position at the detector and normalization.

However, this PSF model is valid only for a source with constant flux. If the observed duration of the emission is significantly shorter than the transit duration (i.e. width of the triangular function), the position in the time direction becomes ambiguous. We illustrate the situation schematically in Figure 3. For the case of long duration event (left panels), the peak time of the triangular response can be determined without ambiguity. On the other hand, for the short event (right panels), the peak time can not be determined as unique. We illustrated possible two extreme cases in the panel: the burst is observed at the end (dashed line) or beginning (dash-dotted line) of the triangular response. The true response is somewhere between the two cases. This ambiguity in the peak time reflects the ambiguity in the position of the source.

In such a case, we calculate an error box of the source position based on the ambiguity in time. At first, we calculate the position assuming a constant source (i.e. fit with the PSF for a constant source). We get a systematically small error box in this approach.

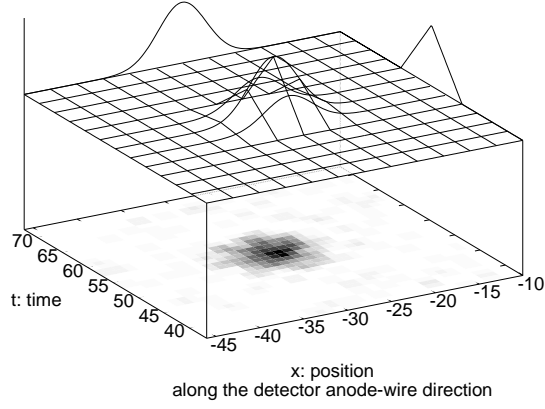


**Fig. 2.** A schematic view of PSF fit of an X-ray source. The bottom map is the observed X-ray image of an X-ray source. We fit the PSF (the above function) to the image. An intersection of the PSF for the direction along the detector anode-wire ( $x$ ) is modeled with a Gaussian. The triangular shape of an intersection of the PSF for the direction along the scan (i.e. time,  $t$ ) reflects the variation of the effective area during the scan. The shape of intersections are also shown in the figure. The free parameters in fitting are position of the peak in the  $x-t$  plane, which corresponds to the position in the celestial coordinate, and the normalization, which corresponds to the source flux.

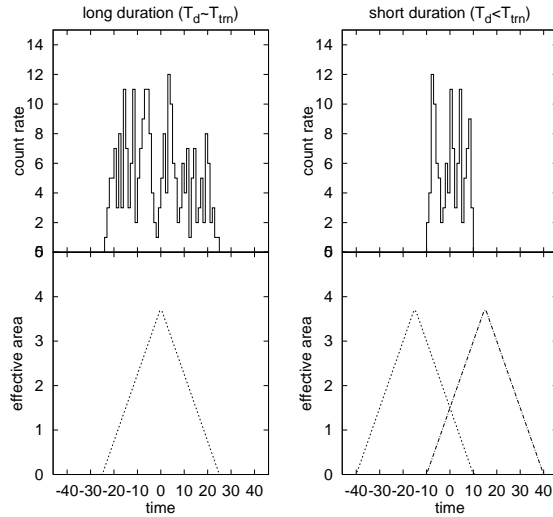


**Fig. 3.** Illustrations of localization ambiguity for a long (left) and short (right) duration events. The solid lines are the simulated observed count rate curves and the dashed lines or the dash-dotted lines are the effective area curves. When the event duration is short, the source position (time) cannot be determined as unique.



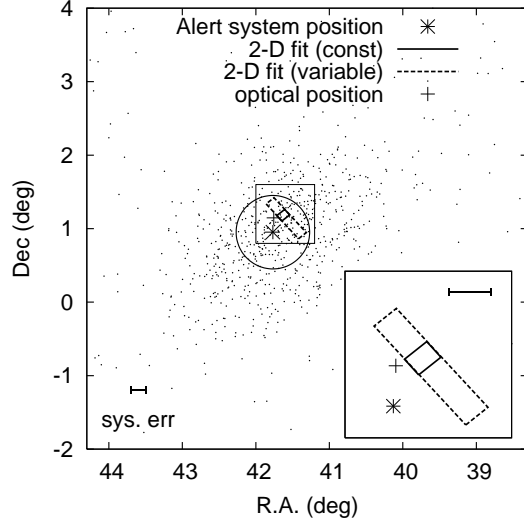


**Fig. 4.** The localization error boxes of GRB 110213B. The dots are position of the X-ray events in the celestial coordinates. The star mark and the circle show the position and the error circle derived by the *MAXI Nova-Alert System*, respectively. The solid and dashed boxes represent the positions derived by two-dimensional (2-D) source fitting, where constant and variable flux of the source are assumed, respectively. The horizontal bars indicate the magnitude of the systematic error for these error boxes. The position of the optical counterpart of this GRB is shown with the plus mark. The square region is expanded in the inset.

Next, we extend the error box taking into account the ambiguity in the scan (time) direction. The size of the error in this direction is  $\delta\theta(T_{\text{trn}} - T_d)/T_{\text{trn}}$ , where  $\delta\theta$ ,  $T_{\text{trn}}$ , and  $T_d$  are the PSF size in the scan direction, the duration of the transit, and the observed duration of the burst, respectively.

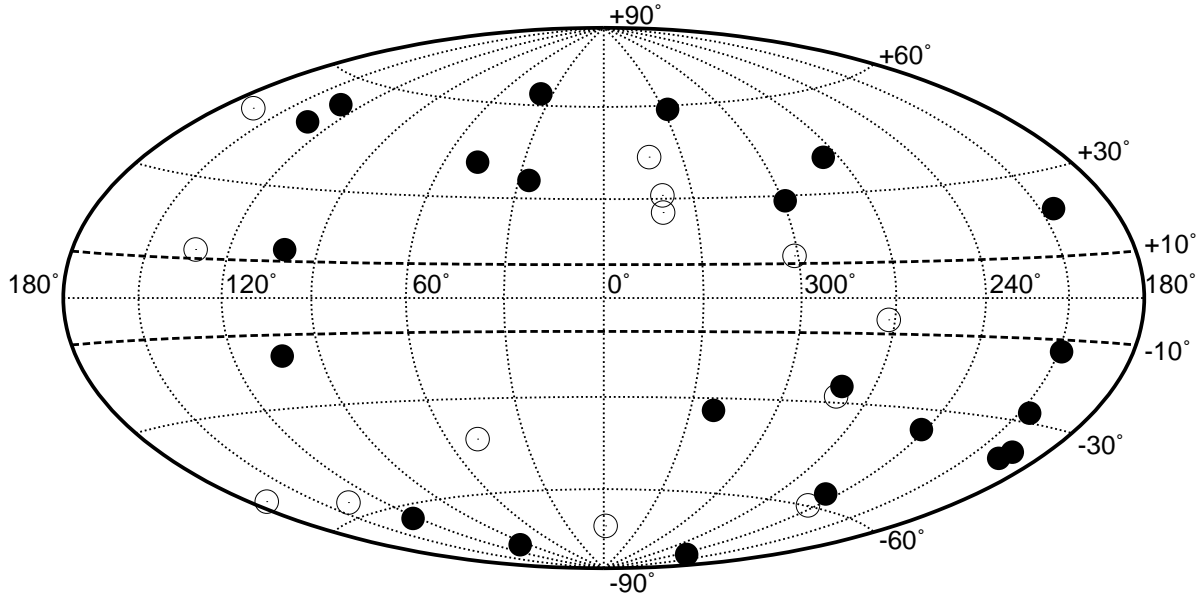
There are additional 0.1 deg systematic errors in the position determination (Morii et al., 2011)<sup>1</sup>.

Figure 4 shows an example of localization error circles and boxes of GRB 110213B. The small solid error box is the result of a fit under the assumption of PSF of a constant source. If we consider the shortness of the detection time, the error box is extended toward the direction of the scan, resulting in the dashed one.

The position determined only by the MAXI data is all consistent with the optical counterpart position by taking into account the systematic error. Figure 5 shows the all-sky map of the MAXI GRBs.

<sup>1</sup> When the paper was written, the systematic error was 0.2 deg. After the additional position calibration, the systematic error has been reduced to 0.1 deg.





**Fig. 5.** An all-sky map of MAXI GRBs in the galactic coordinates. The open circles are the position of the GRBs also observed by other satellites. The filled circles are the position of the GRBs observed only by MAXI. The thick dashed lines are at the galactic latitude  $b = \pm 10^\circ$ , where we excluded the events (see text for the details).

## 2.4. Light curves of the bursts

### 2.4.1. Light curves of MAXI bursts

To create light curves of MAXI bursts, we have to select the source region in the image. In order to reduce systematic background variation, we adopted the data selection using detector coordinates, rather than celestial coordinates. We selected the region that the separation of the source-acquisition angle, which is the angle with respect to the orbital plane of MAXI (Mihara et al., 2011), from the position of the source is  $|\delta\beta| \leq 1.5^\circ$ . The selected region projected to the celestial coordinate forms a belt-like shape region with the width of  $3^\circ$ .

The light curves of MAXI data are as a result of a convolution of the source variation and a change of an effective area. In order to see the intrinsic source variation, we divide the observed counts by the effective area at the time. However, if a duration of an event is shorter than a transit time, a position of a source cannot be determined as mentioned in the previous section. In such a case, the effective area and a flux variation of a source may also be ambiguous.

The left panels of figure 6 show samples of light curves of GRB 091120 observed by MAXI, comparing with those of Fermi/GBM (Meegan et al., 2009). According to the light curves of Fermi/GBM, the duration of this burst is much longer than the transit time. Therefore the localization error is relatively small. We corrected the MAXI light curves with the effective

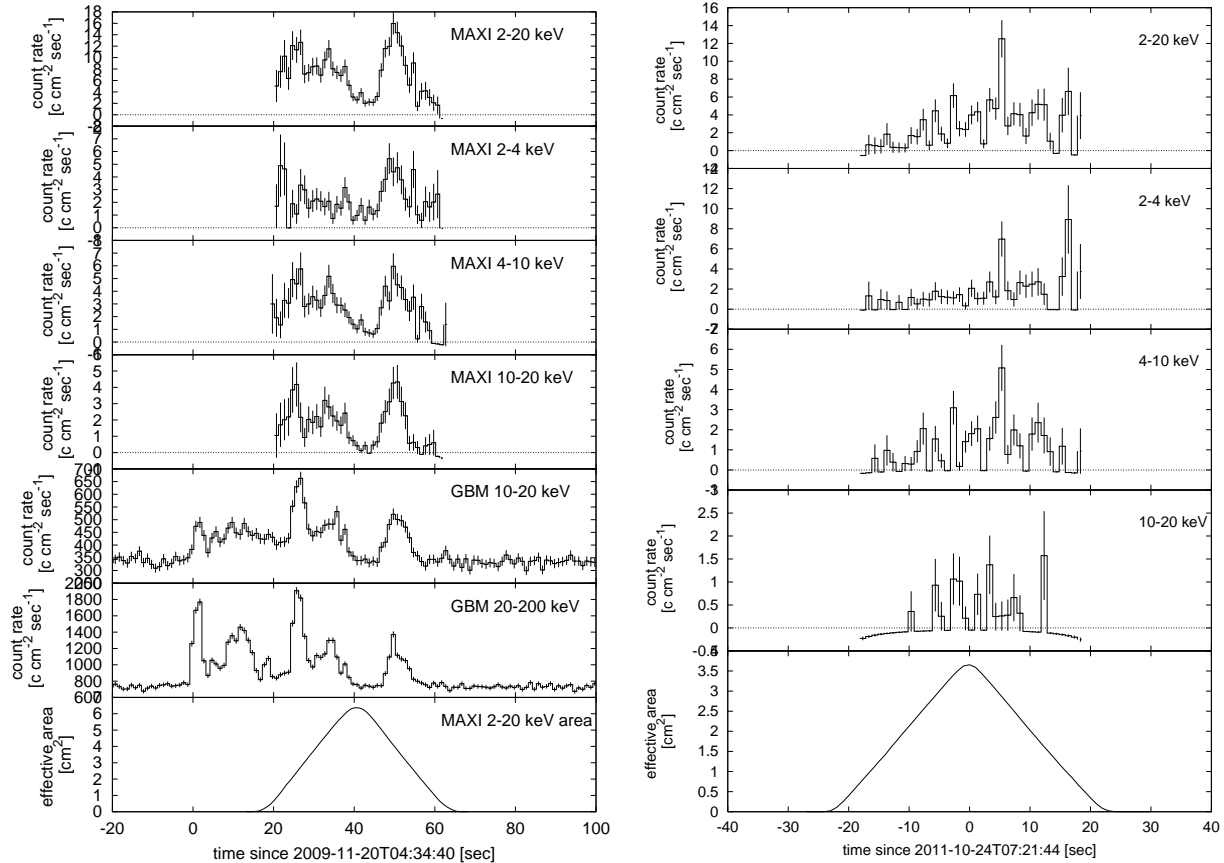


**Fig. 6.** Light curves of GRB 091120 (left) and GRB 111024A (right). The light curves of MAXI are corrected with the effective area of each energy band. For GRB 091120, the light curves observed by Fermi/GBM are also plotted for comparison. Effective area curves are shown in the bottom panels.

area of each energy band. Note that we assumed the photon index of  $-2$  when we calculate the effective area. The right panels of figure 6 shows the light curves of GRB 111024A, which is not observed by other satellites. The light curves are variable like classical GRBs. However, most of MAXI bursts are not so bright to observe the variability. The light curves of all MAXI bursts presented in this paper are available on the MAXI web page<sup>2</sup>.

#### 2.4.2. Hardness and intensity analyses

Because the effective area of GSC can only achieve typically  $\sim 10 \text{ cm}^2$ , GSC usually does not have enough photons to perform spectral analysis for short-lived events. Therefore we decided to study two parameters, the average energy flux and the hardness ratio, which are possible to derive without performing spectral analysis with a relatively small assumption.

The hardness ratio is defined as the ratio of photon flux in 8–20 keV band to that in 2–8 keV band, assuming a spectral slope  $-2^3$ . In order to calculate the average flux in the unit of

<sup>2</sup> <http://maxi.riken.jp/grbs>

<sup>3</sup> We re-calculate the hardness using the spectral slope estimated from the hardness. However, the change

ergs cm<sup>-2</sup> s<sup>-1</sup>, first we calculated the average photon flux in the 2–20 keV band. The average photon flux is determined as the total counts of the bursts in the 2–20 keV band divided by the total effective area times the scan duration around the burst. The background count rate is calculated from the count rate before and after the transit. After the background subtraction, the total counts of the burst is calculated as the observed count during the transit.

To obtain reliable energy flux, we took into account the spectral hardness of the burst in calculating the effective area. We calculated a photon index in the simple power-law model from the observed hardness ratio. Then the photon flux is converted into the energy flux using this estimated photon index.

The uncertainty in the flux measurement comes not only from statistical error but also from systematic uncertainty of the effective area. The degree of this systematic uncertainty depends on the ratio of the observed duration of the burst  $T_d$  to the duration of the transit  $T_{\text{trn}}$ . Since MAXI may not observe a whole GRB,  $T_d$  does not mean usual “duration” (like  $T_{90}$ ), but it means the lower limit of the duration. In the case of  $T_d/T_{\text{trn}} \geq 0.5$ , the maximum uncertainty is 1.5 (i.e. the flux is underestimated and the true flux can be 1.5 higher than that of calculated from MAXI data). If  $T_d/T_{\text{trn}} < 0.5$ , the maximum uncertainty in flux can be expressed as

$$\frac{T_{\text{trn}}}{T_d} - \frac{1}{2},$$

which becomes larger for the shorter burst.

In addition, there is possibility that the average flux here is different from the average flux observed by other satellites. This is because MAXI may observe only a part of long GRB. In fact, GRB 120711 became 5 times brighter than the flux at the time of MAXI observation after the end of MAXI transit. So, the average flux here should be treated with care.

The flux and hardness parameters are summarized in table 3. Figure 7 shows the relationship between the hardness ratio and the time-averaged flux. The bursts only observed by MAXI (“only MAXI”, triangles) tend to distribute at the soft and the low flux region (lower left part of the plot). On the other hand, most of the bright ( $> 10^{-8}$  ergs cm<sup>-2</sup> s<sup>-1</sup>) bursts, which were also observed by other instruments simultaneously (“simul.-GRBs”, circles), show relatively hard spectra. From this figure, we conclude MAXI/GSC is generally sensitive to soft and dim bursts. Averages of the hardness of “only MAXI” and “simul.-GRBs” are 0.32 and 0.54, respectively.

### 2.5. Spectral analyses

We selected bright GRBs with high S/N ( $>35$ ) to have an enough statistics to perform spectral analysis. There are 7 GRBs which satisfy this criterion. If the bursts are simultaneously observed by Swift/BAT (Barthelmy et al., 2005) or Fermi/GBM (Meegan et al., 2009), we performed joint spectral fit of the MAXI spectrum and the spectrum of those instruments. The

---

due to the assumed spectral slope is smaller than the statistic error of the hardness

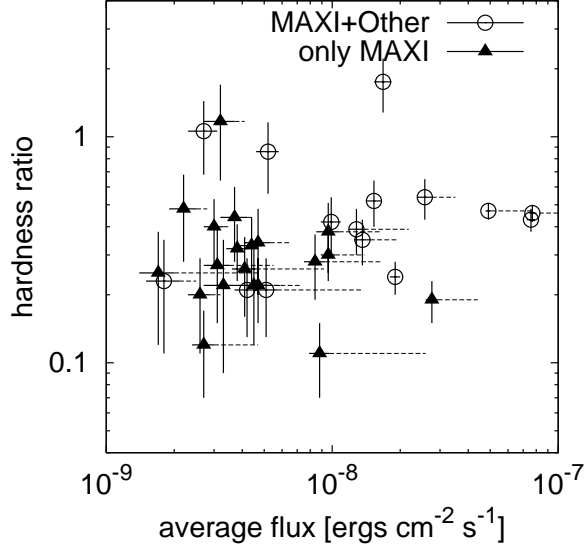


**Fig. 7.** Flux and hardness of MAXI GRBs. The bursts which were also observed by other instruments are plotted with circles (simul.-GRBs). The bursts which were not observed by other instruments are plotted with triangles. The solid error bars correspond to the statistic errors and the dashed error bars on the average flux correspond to the systematic errors.

spectrum of those high energy instruments is useful to constrain the broad-band spectral shape of GRBs. Since the MAXI transit time is rather short, the entire GRB episode can extend beyond the transit time. In these cases, we truncated the data of other missions into the same start and end time as MAXI’s transit time for the spectral analyses.

We analyzed the time averaged spectra of 7 GRBs. Four of them are jointly fitted with the GBM or the BAT data. We tested three type of models: power-law (PL), power-law with exponential cutoff (CPL), and GRB model (GRBM) (so-called Band Function; Band et al., 1993). When we perform the spectral analyses without the GBM or the BAT data, the  $E_{\text{peak}}$  may converge at an inappropriate value due to the limitation of the GSC energy range. In such a case, we calculated lower limit of  $E_{\text{peak}}$  at 90% confidence by fixing a low energy photon index  $\alpha$  to  $-1.0$ . When a high energy photon index  $\beta$  is not well constrained, we fix the index  $\beta$  to  $-2.3$ . We do not consider these models with artificially fixed parameters as the best fit models. The results are summarized in table 4. All the errors in the table are in 90% confidence. Although the S/N of GRB 090926B is lower than our criteria, we also listed the spectral parameters of GRB 090926B in the table, because they are already given by Serino et al. (2011). The  $E_{\text{peak}}$  of the MAXI-Fermi GRBs are 60–100 keV range. While the  $E_{\text{peak}}$  of the MAXI-Swift and MAXI GRBs may be located below 20 keV.

### 3. Discussions

#### 3.1. GRB rate and detection sensitivity

Conventional studies of GRB rate are targeted on relatively high energy band. For example, Stern et al. (2002) made a  $\log N - \log P$  curve in the 50–300 keV band using BATSE and *Ulysses* samples. Suzuki & MAXI Team (2009) estimated that the detection limit of MAXI/GSC is equivalent to 0.4 photons  $\text{cm}^{-2} \text{s}^{-1}$  in the 50–300 keV band based on the simulation study. The corresponding rate is about 400 GRBs per year. An average observing efficiency of MAXI/GSC is about 40% and sky coverage is about 2% of the whole sky. Multiplying these numbers, we expect  $\sim 3$  events per year for the MAXI GRB rate. However we have observed 35 event in 44 months, which is more than three times higher than this estimation. Interestingly, the rate of “simul.-GRB” is close to the expected rate. Since the two thirds of MAXI GRBs are probably not observed by other satellites, those MAXI GRBs are not included in the calculation of the expected number by Suzuki & MAXI Team (2009). According to figure 7, most of GRBs in hardness  $> 0.4$  are “simul.-GRB”. On the other hand, “only MAXI” bursts dominate the range of hardness  $< 0.4$  and also tend to be underluminous. Therefore, it is reasonable that GRB rate expected from the  $\log N - \log P$  based on BATSE and *Ulysses* samples does not agree with the observed rate in the MAXI/GSC energy band. This fact suggests that there are many soft bursts failed to be detected by the traditional GRB instruments.

There is a convincing evidence of existence of soft and underluminous GRBs. According to Meegan et al. (2009), Fermi/GBM operates 90 % of the time. About 50 % of MAXI events are occulted by the Earth for Fermi/GBM. We confirmed that 17 out of 35 MAXI GRBs were inside the Fermi/GBM FOV and not occulted by the Earth. However, only 7 GRBs are detected by Fermi/GBM. Thus, for the other 10 events, we analyzed the daily monitoring CSPEC data, which are publicly available in Fermi Science Support Center web page<sup>4</sup>. We can not find any significant signal around MAXI trigger time for all those 10 events. Figure 8 shows the flux and hardness of the GRBs with or without Fermi/GBM detection. GRB 110426A and GRB 120908A, plotted with triangles, were also triggered by GBM, but the trigger time were before the MAXI observations (cf. table 1). At the time of MAXI observation, the signal in the GBM data is not apparent. There is clear trend in the figure. Fermi/GBM detected bright and hard events among the MAXI GRBs.

GRB 101117A was in the FOV of Swift/BAT, but no significant signal was seen in the BAT data. For Suzaku/WAM (Yamaoka et al., 2009), only GRB 090831 has been detected. Out of the other 34 GRBs, 19 were not occulted by the Earth nor occurred during the off time. Based on those studies, we concluded that large fraction of MAXI GRBs are not detectable by the traditional GRB instruments.

---

<sup>4</sup> <http://fermi.gsfc.nasa.gov/ssc/>

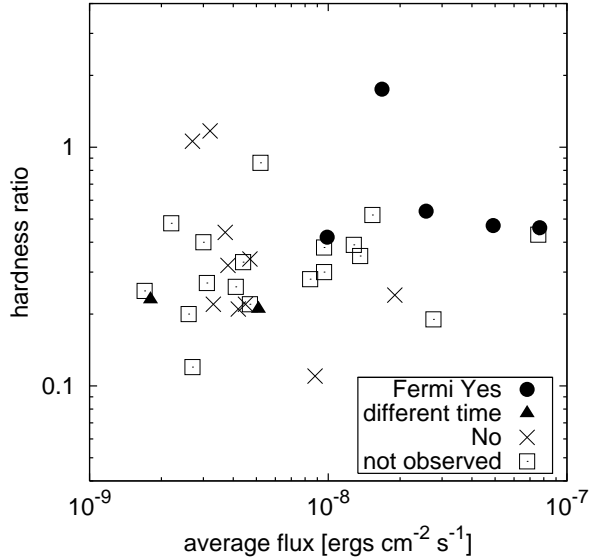


**Fig. 8.** Flux and hardness of MAXI GRBs with or without Fermi/GBM detection. The bursts which are also observed by GBM are plotted with circles. Two events shown by triangles were detected by GBM, but the trigger time were not during the MAXI transit (see text). The bursts shown with cross marks were observed but no significant signal is found. The bursts shown with squares were not observed (occulted or occurred during the off time) by GBM.

In order to compare the results with observations in similar energy range, we plotted histograms of flux and hardness distribution of GRBs observed by HETE-2/WXM (Sakamoto et al., 2005) in figure 9. From the left panel, we see that the average flux of the MAXI bursts are systematically lower than that of the WXM GRBs. Although the effective area of GSC is 3–6 times smaller than that of WXM, the slit and collimator optics of GSC makes the background lower and thus achieves higher sensitivity than WXM. The right panels of figure 9 show the distribution of the hardness of the MAXI and the HETE samples. The hardness distribution of the MAXI GRBs, especially “only MAXI” bursts, has a similar trend to that of the HETE XRFs. We can compare the mean hardness value of each GRB class. the HETE XRFs, X-ray rich GRBs, and classical GRBs have the mean hardness of 0.29, 0.49, and 0.75, respectively. The mean hardness of “only MAXI” bursts is 0.32, and it is the nearest to the HETE XRFs.

### 3.2. Spectral properties of MAXI bursts

MAXI has unique capability to observe soft GRBs. In HETE-2 samples, about one third of GRBs is classified into XRFs (Sakamoto et al., 2005). Although it is difficult to classify GRBs solely from the MAXI data, we expect that roughly one third of the MAXI GRBs are classified into XRFs on the basis of the similarity between the distributions of the hardness of MAXI and HETE bursts.

A traditional parameter  $E_{\text{peak}}$ , is used to represent the softness of GRBs. However,

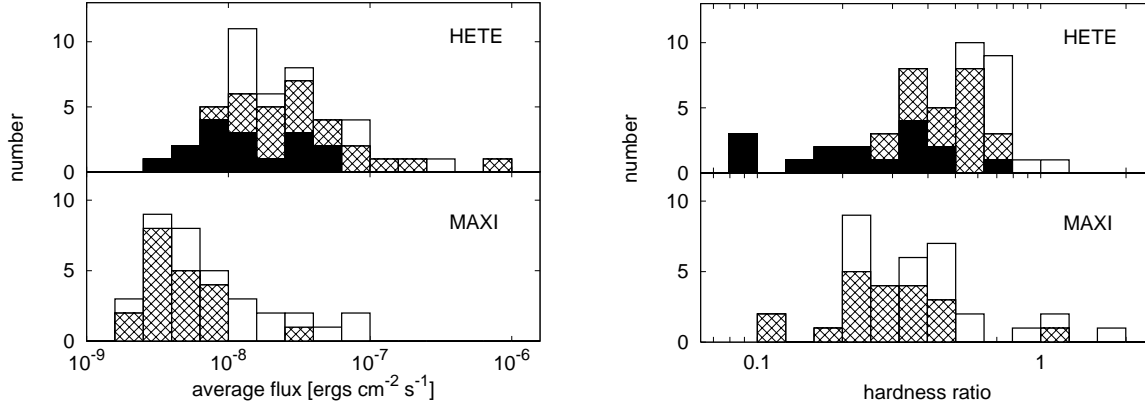


**Fig. 9.** Histograms of time-averaged flux in the 2-20 keV band (left) and hardness (right) distribution of MAXI and HETE-2 GRBs. The hardness is defined as the ratio of photon flux in the 8–20 keV band to the 2–8 keV band. The histograms of top panels are result of HETE-2/WXM (Sakamoto et al., 2005). The histograms of MAXI/GSC are plotted in the bottom panels. The GRBs observed by HETE-2 are classified into (classical) GRBs (open), X-ray rich GRBs (hatched), and X-ray flashes (filled). The hatched bursts in the bottom panels are “only MAXI” bursts.

only a few bursts have enough statistics for spectral analysis in the MAXI samples. Instead of  $E_{\text{peak}}$  we calculated hardness of the bursts (section 2.4.2). In order to examine the relationship between the  $E_{\text{peak}}$  and the hardness, we calculated the hardness ratio in the MAXI energy bands, photon flux in the 8–20 keV band to the 2–8 keV band, using the Band function with fixed indices  $\alpha = -1.0$  and  $\beta = -2.3$ . The result is shown in figure 10. According to Kaneko et al. (2006), the distributions of indices  $\alpha$  and  $\beta$  have deviation of  $\sim 0.3$ . Considering this deviations, we also plotted the curves of a harder ( $\alpha = -0.7$ ,  $\beta = -2.0$ ) and a softer ( $\alpha = -1.3$ ,  $\beta = -2.6$ ) cases in dashed lines. In this figure, we also plotted the best-fit  $E_{\text{peak}}$  or its lower limits of 8 MAXI GRBs shown in table 4. Although the uncertainty of the  $E_{\text{peak}}$  obtained from the spectral analyses are large, they are consistent with the  $E_{\text{peak}}$  inferred from the hardness. The exception is GRB 090926B locating right with hardness  $> 1$ . Since the spectral index  $\alpha$  of this burst is positive (Serino et al., 2011) and far from the assumed value  $-1$ , it is not surprising that this GRB does not follow the relationship.

In figure 9, we see most of the “only MAXI” events have hardness  $< 0.4$ . According to figure 10, the hardness of  $< 0.4$  corresponds to  $E_{\text{peak}} < 20$  keV. Since all the bursts which have  $E_{\text{peak}} < 20$  are classified to XRFs (Sakamoto et al., 2005, 2008), most of the “only MAXI” events can be classified as XRFs.

### 3.3. What does MAXI observe?

An essential question is whether the “only MAXI” events are XRFs or other transient phenomena. A reliable way to answer the question is to carry out follow-up observations of these bursts in other wavelengths. However we have not succeeded them yet. We do not know



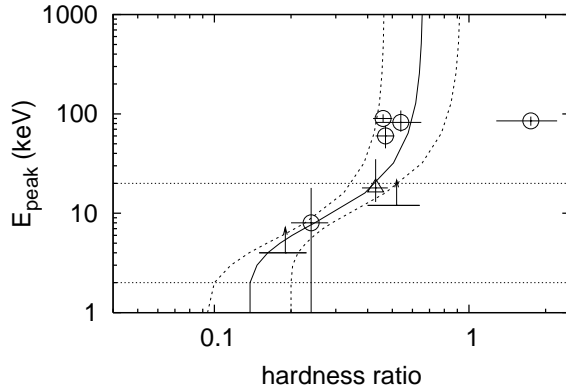


**Fig. 10.** The relation between hardness ratio (8–20 keV/2–8keV) and  $E_{\text{peak}}$  of MAXI GRBs. The solid line shows the correlation calculated with Band function with spectral indices  $\alpha = -1.0$  and  $\beta = -2.3$ . The right and left dashed curves correspond to a harder ( $\alpha = -0.7$ ,  $\beta = -2.0$ ) or a softer ( $\alpha = -1.3$ ,  $\beta = -2.6$ ) spectral models, respectively. The open circles are results from the joint spectral fitting with other instruments. GRB 110213B is plotted with the triangle. For GRB 111024A and GRB 120510A, we cannot obtain reasonable  $E_{\text{peak}}$  without fixing  $\alpha$ . Therefore lower limits calculated with fixed  $\alpha = -1$  are shown with arrows. The horizontal dotted lines show the upper and lower boundaries of GSC energy range used for the hardness calculation.

redshift for any of the “only MAXI” events so far.

Instead of direct study of the distribution of distance to the source, we plotted cumulative distribution of the average flux in figure 11. In the figure, we also indicated the fluxes of four bursts with known redshifts, which are “simul.-GRBs”. The best fit slope to the observed distribution of “simul.-GRBs” becomes flatter than  $-3/2$  below the flux around  $10^{-8}$  ergs  $\text{cm}^{-2} \text{s}^{-1}$ , while the slope of “only MAXI” bursts is close to  $-3/2$  down to the flux range of  $3 \times 10^{-9}$  ergs  $\text{cm}^{-2} \text{s}^{-1}$ . It would suggest that “only MAXI” burst has a uniform distribution down to  $3 \times 10^{-9}$  ergs  $\text{cm}^{-2} \text{s}^{-1}$  and there is no selection effect of the triggering sensitivity above this level. Generally the flattening of the slope from  $-3/2$  at the low flux is interpreted as a cosmological effect (Meegan et al., 1992). Therefore the difference in the slope of “only MAXI” GRBs suggests the intrinsically different population from “simul.-GRBs”. The “only MAXI” GRBs have low luminosity and distribute closer to us than the “simul.-GRBs”. Sakamoto (2004) inferred that XRFs observed by HETE-2 distribute closer distance than hard GRBs, because the slope of the HETE-2  $\log N - \log P$  distribution of XRFs are steeper than that of hard GRBs above 2 photons  $\text{cm}^{-2} \text{s}^{-1}$ . Our MAXI result shows similar trend to the results of HETE-2.

Is there any possibility that “only MAXI” events are galactic transients? In order to investigate whether we can distinguish galactic transients from GRBs by hardness ratio or not, we calculated the hardness of galactic transients assuming their typical emission models. As sources of galactic transients, we considered (type-I) X-ray bursts (XRBs), which are ther-

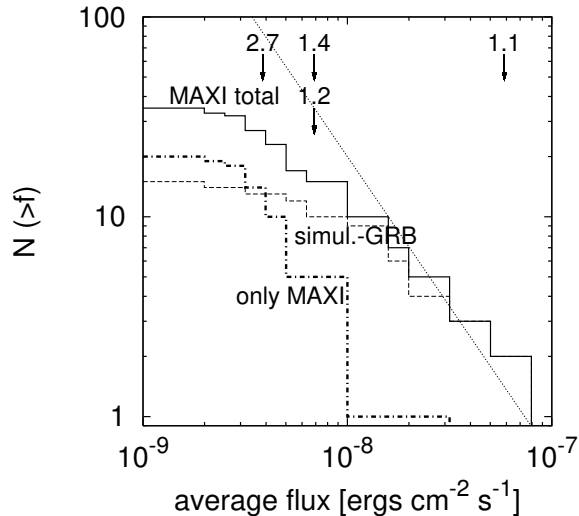


**Fig. 11.** The cumulative distribution of average flux. The solid, dashed, and dash-dotted lines represent the numbers of total, “simul.-GRBs”, and “only MAXI” events, respectively. The dotted line has a slope of  $-3/2$ , indicating a uniform distribution. The arrows show the fluxes of four GRBs with known redshifts. The numbers on the arrows are their redshift values.

monuclear flashes on neutron stars, and stellar flares. We plotted the distribution of hardness of GRBs and galactic transients in figure 12. The hardness range of GRBs is overlapping with those of XRBs or stellar flares. Therefore it is difficult to distinguish between GRBs and XRBs only from the hardness ratio. The most reliable way to distinguish GRBs from XRBs or stellar flares is to refer the catalogs of known sources. However this method is not applicable to a new transient source. An example of such event is an X-ray burst from Swift J1741.5-6548 (Negoro et al., 2013). MAXI detected a burst on 2012 December 25, and the position of the burst did not match with any known X-ray source. We reported the event as GRB 121225A at first (Ogawa et al., 2012). Two months later, Swift detected a previously unknown transient source (Krimm et al., 2013), and the position of the source was marginally consistent with the position of GRB 121225A. If a follow-up observation of GRB 121225A had been performed immediately after the MAXI detection, we would have found the counterpart. We learned the importance of immediate follow-up observations from this example.

There are possibilities of confusing XRBs from previously unknown source like the example of Swift J1741.5-6548 in the MAXI GRB samples. In fact, HETE J1900.1-2455 was not known when HETE-2 detected the first XRB from this object (Vanderspek et al., 2005; Suzuki et al., 2007). Although a persistent emission from the XRB source is expected, MAXI is often not sensitive enough to detect a weak persistent emission. Therefore it is desirable to carry out follow-up observations by a highly sensitive X-ray telescope to find a persistent emission of a MAXI transient event to distinguish GRBs from XRBs.

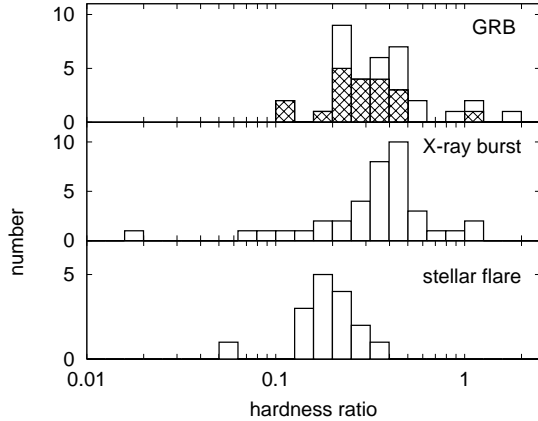


**Fig. 12.** The distribution of the hardness of GRBs, XRBs, and stellar flares observed with MAXI. The hardness is defined as the ratio of photon flux in the 8–20 keV band to the 2–8 keV band. The hatched events in the top panel indicate “only MAXI” bursts.

Unlike GRBs or XRBs, stellar flares have a longer time scale than a scan interval of MAXI. So they are usually observed for multiple scans. Therefore they are easy to be distinguished from GRBs or XRBs. Weak stellar flares may be observed only at the peak due to the sensitivity limit of MAXI. However, the hardness distribution of stellar flares (figure 12) peaks at around the lowest end of the hardness distribution of “only MAXI”. Therefore, we can distinguish the “only MAXI” events from stellar flares by the temporal and the spectral information. We believe that unknown stellar flares are less likely to be confused in our MAXI GRB samples.

#### 4. Conclusion

We selected bright transient events in high ( $> |10^\circ|$ ) galactic latitude from the MAXI/GSC data. We calculated the average energy flux and hardness of these events. The results show that the bursts observed only by MAXI (“only MAXI”) tend to have soft spectra and relatively low flux, comparing to GRBs simultaneously observed by other satellites (“simul.-GRBs”).

In comparison with the GRBs observed by HETE-2/WXM, the average flux of MAXI bursts are lower than those of HETE-2, while the effective area of GSC is 3–6 times smaller than that of WXM. This better sensitivity of GSC comes from its low background, which is a benefit of the slit and collimator optics. From the distributions of the hardness, we found that “only MAXI” bursts have the similar distribution of XRFs observed by HETE-2/WXM.

Since most of MAXI bursts do not have enough statistics to perform spectral analysis, we compared the measured hardness with the calculated hardness assuming the standard GRB spectral parameters. As a result, we found most of the “only MAXI” events have hardness  $< 0.4$ , which corresponds to  $E_{\text{peak}} < 20$  keV.

As of now, there is no “only MAXI” burst with known redshift. The  $\log N - \log S$  slope of “only MAXI” bursts is close to  $-3/2$ , while “simul.-GRBs” show the slope shallower than  $-3/2$ . The difference of the slope of “only MAXI” GRBs suggests that they are intrinsically dim and distribute closer than “simul.-GRBs”.

We looked into a possibility that there was a confusion of galactic transients to the MAXI GRBs. Since the distribution of the hardness of X-ray bursts and stellar flares overlap with those of MAXI GRBs, it is difficult to classify these transients solely by the hardness. The above facts suggest that it is essential to carry out follow-up observations and find counterparts. Direct measurement of redshift distribution and/or identifying a counterparts in other wavelengths are needed to unveil those events.

This research was partially supported by the Ministry of Education, Culture, Sports, Science and Technology (MEXT), Grant-in-Aid No.19047001, 20041008, 20244015, 21340043, 23740147, 24684015, 24740186, and Global-COE from MEXT “Nanoscience and Quantum Physics”.

## References

- Band, D., Matteson, J., Ford, L., et al. 1993, *ApJ*, 413, 281
- Barthelmy, S. D., Barbier, L. M., Cummings, J. R., et al. 2005, *Space Sci. Rev.*, 120, 143
- Bhat, P. N., Chaplin, V., Connaughton, V., & Meegan, C. 2010, GRB Coordinates Network, 10745, 1
- Briggs, M. S. 2009, GRB Coordinates Network, 9957, 1
- Butler, N. R., Bloom, J. S., & Poznanski, D. 2010, *ApJ*, 711, 495
- Cenko, S. B., Prochaska, J. X., Cucchiara, A., Perley, D. A., & Bloom, J. S. 2011, GRB Coordinates Network, 11736, 1
- Chen, H.-W., Helsby, J., Sheckman, S., Thompson, I., & Crane, J. 2009, GRB Coordinates Network, 10038, 1
- D’Alessio, V., Piro, L., & Rossi, E. M. 2006, *A&A*, 460, 653
- Fynbo, J. P. U., Malesani, D., Jakobsson, P., & D’Elia, V. 2009, GRB Coordinates Network, 9947, 1
- Fynbo, J. P. U., Tanvir, N. R., D’Elia, V., et al. 2012, GRB Coordinates Network, 14120, 1
- Golenetskii, S., Aptekar, R., Frederiks, D., et al. 2009a, GRB Coordinates Network, 10189, 1
- Golenetskii, S., Aptekar, R., Frederiks, D., et al. 2009b, GRB Coordinates Network, 9861, 1
- Golenetskii, S., Aptekar, R., Frederiks, D., et al. 2012a, GRB Coordinates Network, 13446, 1
- Golenetskii, S., Aptekar, R., Mazets, E., et al. 2011, GRB Coordinates Network, 11722, 1
- Golenetskii, S., Aptekar, R., Mazets, E., et al. 2012b, GRB Coordinates Network, 13295, 1
- Golenetskii, S., Aptekar, R., Mazets, E., et al. 2012c, GRB Coordinates Network, 13351, 1
- Golenetskii, S., Aptekar, R., Mazets, E., et al. 2013, GRB Coordinates Network, 14135, 1

Gotz, D., Mereghetti, S., Bozzo, E., et al. 2012, GRB Coordinates Network, 13434, 1  
 Gotz, D., Mereghetti, S., Paizis, A., et al. 2009, GRB Coordinates Network, 10298, 1  
 Granot, J., Ramirez-Ruiz, E., & Perna, R. 2005, ApJ, 630, 1003  
 Gruber, D. 2009, GRB Coordinates Network, 10187, 1  
 Gruber, D. & Pelassa, V. 2012, GRB Coordinates Network, 13437, 1  
 Grupe, D., Barthelmy, S. D., Cummings, J. R., et al. 2009, GRB Coordinates Network, 9935, 1  
 Heise, J., Zand, J. I., Kippen, R. M., & Woods, P. M. 2001, in Gamma-ray Bursts in the Afterglow Era, ed. E. Costa, F. Frontera, & J. Hjorth, 16  
 Kaneko, Y., Preece, R. D., Briggs, M. S., et al. 2006, ApJS, 166, 298  
 Krimm, H. A., Holland, S. T., Kennea, J. A., et al. 2013, The Astronomer's Telegram, 4902, 1  
 Lamb, D. Q., Donaghy, T. Q., & Graziani, C. 2005, ApJ, 620, 355  
 Lien, A. Y., Sakamoto, T., Gehrels, N., et al. 2014, in American Astronomical Society Meeting Abstracts, Vol. 223, American Astronomical Society Meeting Abstracts, #352.06  
 Mangano, V., Barthelmy, S. D., Burrows, D. N., et al. 2010, GRB Coordinates Network, 11135, 1  
 Maselli, A., Barthelmy, S. D., Baumgartner, W. H., et al. 2012, GRB Coordinates Network, 14045, 1  
 Matsuoka, M., Kawasaki, K., Ueno, S., et al. 2009, PASJ, 61, 999  
 McGlynn, S. 2012, GRB Coordinates Network, 13741, 1  
 Meegan, C., Lichti, G., Bhat, P. N., et al. 2009, ApJ, 702, 791  
 Meegan, C. A., Fishman, G. J., Wilson, R. B., et al. 1992, Nature, 355, 143  
 Mészáros, P., Ramirez-Ruiz, E., Rees, M. J., & Zhang, B. 2002, ApJ, 578, 812  
 Mihara, T., Nakajima, M., Sugizaki, M., et al. 2011, PASJ, 63, 623  
 Morii, M., Sugimori, K., Kawai, N., & MAXI Team. 2011, Physica E Low-Dimensional Systems and Nanostructures, 43, 692  
 Negoro, H., Serino, M., Ogawa, Y., et al. 2013, The Astronomer's Telegram, 4911, 1  
 Ogawa, Y., Nakahira, S., Serino, M., et al. 2012, GRB Coordinates Network, 14100, 1  
 Ohmori, N., Noda, K., Sonoda, E., et al. 2009, GRB Coordinates Network, 9900, 1  
 Qin, S.-F., Liang, E.-W., Lu, R.-J., Wei, J.-Y., & Zhang, S.-N. 2010, MNRAS, 406, 558  
 Rau, A. 2009, GRB Coordinates Network, 9850, 1  
 Ricker, G. R., Atteia, J.-L., Crew, G. B., et al. 2003, in American Institute of Physics Conference Series, Vol. 662, Gamma-Ray Burst and Afterglow Astronomy 2001: A Workshop Celebrating the First Year of the HETE Mission, ed. G. R. Ricker & R. K. Vanderspek, 3–16  
 Sakamoto, T. 2004, PhD thesis  
 Sakamoto, T., Barbier, L., Barthelmy, S. D., et al. 2006, ApJL, 636, L73  
 Sakamoto, T., Barthelmy, S. D., Baumgartner, W. H., et al. 2011, ApJS, 195, 2  
 Sakamoto, T., Hullinger, D., Sato, G., et al. 2008, ApJ, 679, 570

Sakamoto, T., Lamb, D. Q., Graziani, C., et al. 2004, *ApJ*, 602, 875  
Sakamoto, T., Lamb, D. Q., Kawai, N., et al. 2005, *ApJ*, 629, 311  
Serino, M., Yoshida, A., Kawai, N., et al. 2011, *PASJ*, 63, 1035  
Shirasaki, Y., Kawai, N., Yoshida, A., et al. 2003, *PASJ*, 55, 1033  
Soderberg, A. M., Kulkarni, S. R., Berger, E., et al. 2004, *ApJ*, 606, 994  
Soderberg, A. M., Nakar, E., Cenko, S. B., et al. 2007, *ApJ*, 661, 982  
Sonbas, E., D’Elia, V., Kennea, J. A., et al. 2012, *GRB Coordinates Network*, 14115, 1  
Stern, B. E., Atteia, J.-L., & Hurley, K. 2002, *ApJ*, 578, 304  
Strohmayer, T. E., Fenimore, E. E., Murakami, T., & Yoshida, A. 1998, *ApJ*, 500, 873  
Sugizaki, M., Mihara, T., Serino, M., et al. 2011, *PASJ*, 63, 635  
Suwa, F., Negoro, H., Ozawa, H., & Maxi Team. 2010, in *The First Year of MAXI: Monitoring Variable X-ray Sources*, 63P  
Suzuki, M., Kawai, N., Tamagawa, T., et al. 2007, *PASJ*, 59, 263  
Suzuki, M. & MAXI Team. 2009, in *Astrophysics with All-Sky X-Ray Observations*, ed. N. Kawai, T. Mihara, M. Kohama, & M. Suzuki, 224  
Tam, P. H. T., Li, K. L., & Kong, A. K. H. 2012, *GRB Coordinates Network*, 13444, 1  
Tanvir, N. R., Wiersema, K., Levan, A. J., et al. 2012, *GRB Coordinates Network*, 13441, 1  
Tomida, H., Tsunemi, H., Kimura, M., et al. 2011, *PASJ*, 63, 397  
Tsunemi, H., Tomida, H., Katayama, H., et al. 2010, *PASJ*, 62, 1371  
van der Horst, A. J. & Camero-Arranz, A. 2011, *GRB Coordinates Network*, 12013, 1  
Vanderspek, R., Morgan, E., Crew, G., Graziani, C., & Suzuki, M. 2005, *The Astronomer’s Telegram*, 516, 1  
Virgili, F. J., Zhang, B., Nagamine, K., & Choi, J.-H. 2011, *MNRAS*, 417, 3025  
Wanderman, D. & Piran, T. 2010, *MNRAS*, 406, 1944  
Wiersema, K., Curran, P. A., Krühler, T., et al. 2012, *MNRAS*, 426, 2  
Yamaoka, K., Endo, A., Enoto, T., et al. 2009, *PASJ*, 61, 35  
Yamazaki, R., Ioka, K., & Nakamura, T. 2002, *ApJL*, 571, L31  
Zhang, B. & Mészáros, P. 2002, *ApJ*, 581, 1236

**Table 1.** A summary of GRBs and short X-ray transient observed by MAXI

GRB name	time*	(RA, Dec)		loc. error <sup>†</sup>	cameras <sup>‡</sup>	S/N	trigger <sup>§</sup>	other sat. <sup>  </sup>	delay <sup>#</sup>
090831	2009-08-31 07:37:07	145.4	+51.4	C 60'	2,8	185.3	O	F[-31](1)/K[-33](2)/ W[-31](3)	12h
090926B	2009-09-26 21:55:39	46.3	-39.1	C 60'	1,7	28.3	O	S[+9](4)/F[-10](5)	9h
091012**	2009-10-12 10:25:51	182.82	+63.37	C 12'	0,1,7	14.6	H		
091120	2009-11-20 04:35:20	226.81	-21.79	C 30'	1,7	272.1	O	F[-40](6)/K[-44](7)	97h
091201	2009-12-01 21:48:36	118.6	+16.6	C 24'	3	19.0	M		19h
091230**	2009-12-30 06:27:15	132.91	-53.88	C 21'	2,8	9.2	O	I[+15](8)	
100315A	2010-03-15 17:13:40	74.95	-6.63	B 166'×45'	2,8	8.0	M		14h
100327	2010-03-27 17:08:20	346.03	+42.90	B 58'×28'	1,7	12.4	M		66h
100415A	2010-04-15 03:44:54	7.48	-15.57	B 104'×36'	4	26.6	M		9h
100510A	2010-05-10 19:27:23	355.8	-35.6	B 83'×16'	1	51.2	M	F[-16](9)	24h
100616A	2010-06-16 01:42:17	50.95	-40.62	B 110'×70'	4,5	14.0	M		8h
100701A	2010-07-01 06:54:31	188.86	-34.26	B 122'×21'	5	32.5	M		5h
100823A	2010-08-23 17:25:52	20.70	+5.84	C 7'	4,5	67.4	O	S[-17](10)	95h
100911	2010-09-11 14:58:24	103.41	-70.43	B 39'×15'	1,2	8.7	H		41h
101117A	2010-11-17 07:32:57	89.63	-2.30	B 38'×22'	0	28.4	M		3h
101210**	2010-12-10 03:38:27	61.66	-5.36	C 20'	4,5,B	8.8	M		
110213B	2011-02-13 14:32:08	41.76	+1.15	B 40'×7'	4	139.8	M	K[-35](11)	14h
110402**	2010-04-02 02:33:55	62.52	-3.00	E 30'×20'	0,7	11.6	M		
110426A	2011-04-26 15:08:35	221.18	-10.78	B 262'×16'	4,5	20.2	M	F[-128](12)	9h
110916	2011-09-16 20:33:12	171.68	-17.77	B 77'×19'	2,8	13.8	M		85h
111024A	2011-10-24 07:21:44	221.93	+25.87	B 12'×9'	4	74.8	M		5h
120424A	2012-04-24 16:47:29	23.985	-29.87	C 16'	4,5	17.1	M		19h
120510A	2012-05-10 08:48:06	44.285	+72.850	C 10'	0,7	52.8	M	K(13) <sup>††</sup>	5h
120528B	2012-05-28 18:12:08	77.59	-37.80	B 78'×22'	2,7	26.5	M	K[-20](14)	8h
120528C	2012-05-28 21:20:45	12.93	-0.95	E 48'×36'	4,5	6.9	H		31h
120614A	2012-06-14 05:49:10	312.73	+65.16	C 10'	0,7	33.2	M		2h
120622A	2012-06-22 03:21:51	205.43	-1.71	B 130'×30'	2	12.1	M		2h
120626B	2012-06-26 13:38:12	175.77	+68.50	C 30'	0,7	10.5	M		44h
120711A	2012-07-11 02:45:07	94.703	-71.001	B 65'×13'	2	21.4	M	F[-14](15)/L(16)/ I[-19](17)/K[+49](18)	8h
120908A	2012-09-08 22:35:12	230.64	-25.79	E 28'×19'	4,5	6.2	M	F[-252](19)	11h
121025A	2012-10-25 07:46:30	248.75	+27.73	C 17'	4,5	7.0	M		3h
121209A	2012-12-09 21:59:08	327.02	-7.69	C 24'	4,5	9.4	O	S[+3](20)	111h
121229A	2012-12-29 05:01:09	190.10	-50.59	C 24'	2,7	12.2	O	S[-48](21)	4h
130102B	2013-01-02 04:42:03	309.58	-72.38	C 12'	2	35.3	M	K(22) <sup>††</sup>	25h
130407A	2013-04-07 23:36:57	248.10	+10.51	C 12'	4,5	14.9	M		4h

Notes.

\* The center time of the transit in which the burst was observed

† The size of localization error in arcmin. C, B, and E denote the shape of the error; C: circle (radius), B: rectangular box (length), and E: ellipsoid (long and short radii), respectively. The systematic errors are not included.

‡ Camera-IDs of the cameras that observed the burst. There are 12 cameras, camera 0 – 9, camera A, and camera B.

§ M, O, and H denote that they are found by *the MAXI Nova-Alert System*, the information of other satellites, and Human inspection respectively.|| F : Fermi/GBM, L : Fermi/LAT, S : Swift, I : INTEGRAL, K : Konus-Wind, W : Suzaku/WAM. The numbers in the square brackets are the trigger (or detection) time of the instrument from the time in the ‘time’ column. The reference numbers are in the parentheses. The references are as follows: (1) Rau (2009), (2) Golenetskii et al. (2009b), (3) Ohmori et al. (2009), (4) Grupe et al. (2009), (5) Briggs (2009), (6) Gruber (2009), (7) Golenetskii et al. (2009a), (8) Gotz et al. (2009), (9) Bhat et al. (2010), (10) Mangano et al. (2010), (11) Golenetskii et al. (2011), (12) van der Horst & Camero-Arranz (2011), (13) Golenetskii et al. (2012b), (14) Golenetskii et al. (2012c), (15) Gruber & ~~P~~lassa (2012), (16) Tam et al. (2012), (17) Gotz et al. (2012), (18) Golenetskii et al. (2012a), (19) McGlynn (2012), (20) Maselli et al. (2012), (21) Sonbas et al. (2012), (22) Golenetskii et al. (2013).

# The time delay in sending GCN or ATel.

\*\* not reported to GCN or ATel

††



**Table 2.** X-ray and optical counterparts of MAXI GRBs

GRB name	Band	(RA, Dec)		error	GCN#*	redshift (ref.) <sup>†</sup>
090926B	optical	46.30808	-39.00617	0''5	9944	1.24 (1)
091230	optical	132.91325	-53.89797	0''5	10299	
100823A	optical	20.70429	+5.83511	0''9	11148	
110213B	optical	41.75588	+1.14619		11732	1.083 (2)
120510A	X-ray(?) <sup>‡</sup>	44.04666	+72.88692	4''8	13284	
120711A	optical	94.67850	-70.99911		13430	1.405 (3)
121025A	X-ray	248.38182	+27.67189	3''8	13909	
121209A	optical	326.78733	-8.23508	0''5	14049	2.707 (4)
121229A	optical	190.10121	-50.59430	0''5	14117	

Notes.

\* The number of GCN circular which report the position of X-ray or optical counterparts.

<sup>†</sup> The references are (1) Fynbo et al. (2009), (2) Cenko et al. (2011), (3) Tanvir et al. (2012), (4) Fynbo et al. (2012).

<sup>‡</sup> A candidate afterglow was reported, but not confirmed.

**Table 3.** A summary of the flux and the spectral hardness

GRB name	flux*	hardness <sup>†</sup>	$T_d^{\ddagger}$	other sat. <sup>§</sup>
090831	$4.91 \pm 0.14 + 2.68$	$0.47 \pm 0.04$	41.0	yes
090926B	$1.68 \pm 0.15 -$	$1.75 \pm 0.47$	21.3	yes
091012	$0.38 \pm 0.04 + 0.01$	$0.32 \pm 0.09$	43.4	
091120	$7.69 \pm 0.23 + 2.54$	$0.46 \pm 0.04$	29.4	yes
091201	$0.47 \pm 0.06 + 0.12$	$0.34 \pm 0.14$	42.0	
091230	$0.27 \pm 0.04 -$	$1.06 \pm 0.38$	54.7	yes
100315A	$0.17 \pm 0.03 + 0.27$	$0.25 \pm 0.13$	26.8	
100327	$0.26 \pm 0.03 + 0.03$	$0.20 \pm 0.09$	34.6	
100415A	$0.96 \pm 0.11 + 0.57$	$0.38 \pm 0.13$	23.4	
100510A	$2.57 \pm 0.19 + 0.75$	$0.54 \pm 0.11$	28.0	yes
100616A	$0.37 \pm 0.05 + 0.03$	$0.44 \pm 0.16$	38.7	
100701A	$0.88 \pm 0.09 + 1.62$	$0.11 \pm 0.04$	19.8	
100823A	$1.90 \pm 0.10 -$	$0.24 \pm 0.04$	22.9	yes
100911	$0.30 \pm 0.03 + 0.02$	$0.40 \pm 0.13$	37.4	
101117A	$0.84 \pm 0.09 + 0.73$	$0.28 \pm 0.09$	30.0	
101210	$0.22 \pm 0.03 + 0.03$	$0.48 \pm 0.20$	33.5	
110213B	$7.58 \pm 0.32 -$	$0.43 \pm 0.05$	28.4	yes
110402	$0.44 \pm 0.05 + 0.00$	$0.33 \pm 0.11$	53.0	
110426A	$0.51 \pm 0.06 + 0.79$	$0.21 \pm 0.08$	17.3	yes
110916	$0.27 \pm 0.03 + 0.17$	$0.12 \pm 0.05$	43.7	
111024A	$2.76 \pm 0.17 + 1.48$	$0.19 \pm 0.04$	23.6	
120424A	$0.47 \pm 0.05 + 0.08$	$0.22 \pm 0.07$	32.9	
120510A	$1.53 \pm 0.12 -$	$0.52 \pm 0.12$	18.8	yes
120528B	$1.28 \pm 0.10 + 0.80$	$0.39 \pm 0.09$	23.5	yes
120528C	$0.32 \pm 0.05 + 0.04$	$1.17 \pm 0.53$	36.0	
120614A	$0.96 \pm 0.07 + 0.36$	$0.30 \pm 0.07$	29.5	
120622A	$0.45 \pm 0.06 + 0.21$	$0.22 \pm 0.10$	36.0	
120626B	$0.31 \pm 0.04 + 0.20$	$0.27 \pm 0.12$	23.7	
120711A	$0.99 \pm 0.10 -$	$0.42 \pm 0.12$	46.7	yes
120908A	$0.18 \pm 0.03 + 0.04$	$0.23 \pm 0.12$	33.1	yes
121025A	$0.33 \pm 0.06 -$	$0.22 \pm 0.13$	14.6	
121209A	$0.52 \pm 0.06 -$	$0.86 \pm 0.30$	59.0	yes
121229A	$0.42 \pm 0.05 -$	$0.21 \pm 0.08$	32.7	yes
130102B	$1.36 \pm 0.11 + 0.49$	$0.35 \pm 0.08$	44.0	yes
130407A	$0.41 \pm 0.05 + 0.46$	$0.26 \pm 0.10$	19.5	

Notes.

\* In the unit of  $10^{-8}$  ergs  $\text{cm}^{-2}$   $\text{s}^{-1}$  in 2–20 keV. The first error is statistic error and the second error is systematic error due to the uncertainty of the effective area. For a burst with accurate position, the systematic error is negligible.

† Ratio of the photon flux in 8–20 keV to 2–8 keV

‡ The observed duration, which means the lower limit of the real duration of the burst, in the unit of s.

§ The bursts also observed by other satellites are marked

**Table 4.** A summary of the spectral parameters and the flux

GRB name	joint	model	$\alpha$	$\beta$	$E_{\text{peak}}$	flux*	$\chi^2(\text{DoF})$
090831	Fermi	PL	$-1.62^{+0.02}_{-0.02}$	—	—	$(3.95^{+0.12}_{-0.11})$	456.23(261)
		CPL	$-1.27^{+0.04}_{-0.04}$	—	$161^{+27}_{-20}$	$4.73^{+0.15}_{-0.19}$	349.23(260)
		GRBM <sup>†</sup>	$-1.03^{+0.11}_{-0.08}$	$-1.78^{+0.06}_{-0.06}$	$60^{+16}_{-15}$	$5.06^{+0.10}_{-0.25}$	312.60(259)
090926B <sup>‡</sup>	Fermi	CPL	$0.44^{+0.14}_{-0.13}$	—	$97^{+7}_{-6}$	$1.60^{+0.04}_{-0.03}$	93.26(83)
		GRBM <sup>†</sup>	$0.65^{+0.22}_{-0.18}$	$-2.51^{+0.29}_{-0.49}$	$85^{+9}_{-9}$	$1.62^{+0.13}_{-0.18}$	83.13(82)
091120	Fermi	PL	$-1.56^{\S}$	—	—	$(7.60^{\ddagger})$	417.23(76)
		CPL <sup>†</sup>	$-1.15^{+0.06}_{-0.05}$	—	$90^{+9}_{-7}$	$5.72^{+0.19}_{-0.22}$	126.71(75)
		GRBM	$-1.14^{+0.06}_{-0.06}$	$-2.3$ (fixed)	$83^{+10}_{-9}$	$7.23^{+0.32}_{-0.22}$	135.74(75)
100510A	Fermi	PL	$-1.58^{+0.04}_{-0.05}$	—	—	$2.54^{+0.24}_{-0.24}$	85.15(48)
		CPL <sup>†</sup>	$-1.19^{+0.14}_{-0.13}$	—	$82^{+26}_{-16}$	$2.51^{+0.24}_{-0.29}$	46.87(47)
		GRBM	$-1.19^{+0.16}_{-0.13}$	$-2.3$ (fixed)	$78^{+29}_{-20}$	$2.52^{+0.44}_{-0.24}$	48.27(47)
100823A	Swift	PL	$-2.06^{+0.06}_{-0.06}$	—	—	$1.99^{+0.15}_{-0.13}$	53.88(51)
		CPL <sup>†</sup>	$-1.95^{+0.15}_{-0.05}$	—	$8^{+10}_{-8}$	$2.02^{+0.15}_{-0.17}$	51.58(50)
		GRBM	$-1.88^{+0.36}_{-0.23}$	$-2.3$ (fixed)	$10^{+7}_{-9}$	$2.04^{+2.13}_{-2.00}$	50.95(50)
110213B	NA	PL	$-1.17^{+0.10}_{-0.10}$	—	—	$8.12^{+0.63}_{-0.56}$	22.77(21)
		CPL <sup>†</sup>	$-0.53^{+0.44}_{-0.39}$	—	$18^{+17}_{-5}$	$8.34^{+0.17}_{-5.25}$	14.49(20)
111024A	NA	PL <sup>†</sup>	$-2.14^{+0.18}_{-0.20}$	—	—	$3.11^{+0.34}_{-0.33}$	18.71(21)
		CPL	$-1.00$ (fixed)	—	$> 4$	$2.95^{+0.31}_{-0.53}$	16.86(21)
120510A	NA	PL <sup>†</sup>	$-1.30^{+0.25}_{-0.27}$	—	—	$1.20^{+0.24}_{-0.20}$	15.43(18)
		CPL	$-1.00$ (fixed)	—	$> 12$	$1.19^{+0.18}_{-1.19}$	14.04(18)

Notes.

\* in the unit of  $10^{-8}$  ergs  $\text{cm}^{-2}$   $\text{s}^{-1}$  in 2–20 keV

<sup>†</sup> The best fit models for each burst are marked.

<sup>‡</sup> The parameters are from Serino et al. (2011).

<sup>§</sup> The errors are not available.